AD-A126 355 MATERIALS AND ELECTRONIC EQUIPMENT CORROSION TESTS IN SOME US NAVY GEOTHERMAL ENVIRONMENTS(U) NAVAL WEAPONS CENTER CHINA LAKE CA S FINNEGAN ET AL. MAR 83 1/1

UNCLASSIFIED NWC-TP-6393 F/G 11/6 NL

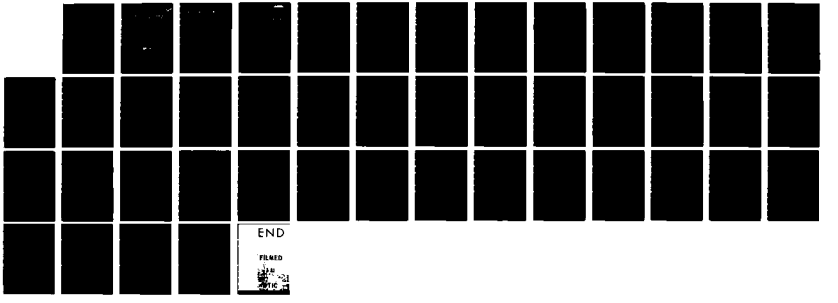

END

FILMED

DTIC

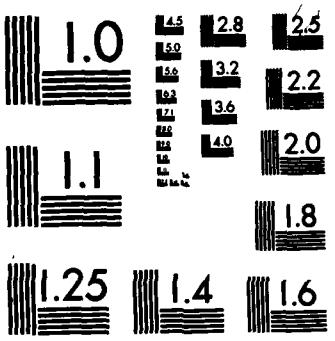

MICROCOPY RESOLUTION TEST CHART
NATIONAL BUREAU OF STANDARDS-1963-A

NWC TP 6393

12

Materials and Electronic Equipment Corrosion Tests in Some U.S. Navy Geothermal Environments

by

C. Rodgers
Public Works Department

S. Finnegan
and
K. Graham
Research Department

MARCH 1983

NAVAL WEAPONS CENTER
CHINA LAKE, CALIFORNIA 93555

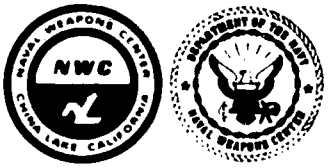

Approved for public release; distribution unlimited.

Naval Weapons Center
AN ACTIVITY OF THE NAVAL MATERIAL COMMAND

FOREWORD

This report describes the corrosion testing conducted between February 1978 and December 1980 on structural materials in geothermal fluids at the Coso Geothermal Area and at the Naval Air Station, Fallon, Nev., and also the environmental testing of aircraft electronic and electrical equipment in a geothermal emissions area at Coso. The investigation, funded under Naval Civil Engineering Laboratory, is a continuing effort to determine the effects of geothermal development on structural and military equipment.

This report was reveiwed for technical accuracy by Carl F. Austin and Dave Stevens.

Released for publication by
B. W. HAYS
Technical Director
8 March 1983

Under authority of
J. J. LAHR
Capt., U.S. Navy
Commander

NWC Technical Publication 6393

Published by ..... Research Department
Collation ..... Cover, 20 leaves
First printing ..... 165 unnumbered copies

UNCLASSIFIED

SECURITY CLASSIFICATION OF THIS PAGE (When Data Entered)

REPORT DOCUMENTATION PAGE		READ INSTRUCTIONS BEFORE COMPLETING FORM
1. REPORT NUMBER NWC TP 6393	2. GOVT ACCESSION NO.	3. RECIPIENT'S CATALOG NUMBER
4. TITLE (and Subtitle) Materials and Electronic Equipment Corrosion Tests in Some U.S. Navy Geothermal Environments		5. TYPE OF REPORT & PERIOD COVERED A summary report Feb 1978-Dec 1980 6. PERFORMING ORG. REPORT NUMBER
7. AUTHOR(s) S. Finnegan, C. Rodgers, and K. Graham		8. CONTRACT OR GRANT NUMBER(s)
9. PERFORMING ORGANIZATION NAME AND ADDRESS Naval Weapons Center China Lake, CA 93555		10. PROGRAM ELEMENT, PROJECT, TASK AREA & WORK UNIT NUMBERS Naval Civil Engineering Laboratory Z0829
11. CONTROLLING OFFICE NAME AND ADDRESS Naval Weapons Center China Lake, CA 93555		12. REPORT DATE March 1983 13. NUMBER OF PAGES 38
14. MONITORING AGENCY NAME & ADDRESS(if different from Controlling Office)		15. SECURITY CLASS. (of this report) 15a. DECLASSIFICATION/DOWNGRADING SCHEDULE

16. DISTRIBUTION STATEMENT (of this Report)

Approved for public release; distribution unlimited.

17. DISTRIBUTION STATEMENT (of the abstract entered in Block 20, if different from Report)

18. SUPPLEMENTARY NOTES

19. KEY WORDS (Continue on reverse side if necessary and identify by block number)

Corrosion, metals
Corrosion, electronic equipment
Geothermal emissions

20. ABSTRACT (Continue on reverse side if necessary and identify by block number)

See back of form.

DD FORM 1 JAN 73 1473 EDITION OF 1 NOV 65 IS OBSOLETE
S/N 0102-LF-014-6601

UNCLASSIFIED

SECURITY CLASSIFICATION OF THIS PAGE (When Data Entered)

(U) ***Materials and Electronic Equipment Corrosion Tests In Some U.S. Navy Geothermal Environments***, by S. Finnegan, K. Graham, and C. Rodgers. China Lake, Calif., Naval Weapons Center, March 1983. 38 pp. (NWC TP 6393, publication UNCLASSIFIED.)

(U) This report documents the results of geothermal corrosion studies conducted at the Coso Geothermal Area, Naval Weapons Center (NWC), China Lake, Calif., and the Naval Air Station (NAS), Fallon, Nev. At the Coso Goethermal Area, five different metallic and nonmetallic materials in tubular shapes were tested for approximately 17 months in two different types of low-pressure, medium-temperature steam environments. In addition, a variety of electronic equipment including aircraft instrumentation and battery-powered test circuits were exposed to a hydrogen-sulfide-rich environment at the Devils Kitchen area for approximately 2 years. At NAS, Fallon, standard corrosion coupons of 11 different metals and alloys and some plastic cement samples were exposed to fluids in a deep brine well for three different time intervals up to 109 days (a planned-interval test series). Exposed samples were analyzed using a variety of methods including optical microscopy, x-ray diffraction techniques, and weight-loss measurements. Corrosion rates, modes, and various corrosion products and precipitates were established for the individual coupons and the tubular specimens, while the electronic instruments and test circuitry were given an operational and bench test before and after exposure and were also visually inspected. Test circuits (and one electronic instrument) were also periodically removed and tested. Results of these three different test programs are discussed individually and recommendations made.

A

TABLE OF CONTENTS

TABLE OF CONTENTS (Contd.)

SECTION I. CONSTRUCTION GRADE MATERIALS TESTING IN NWC COSO AREA GEOTHERMAL STEAM ENVIRONMENTS

INTRODUCTION

Corrosion studies of common construction-grade piping materials in natural geothermal environments have been previously conducted at the Naval Weapons Center (NWC) (Ref. 1). Ten-foot-long sections of nine different materials were exposed to three different moderate-temperature (less than 220°F) geothermal fluids under both anaerobic and aerated conditions for periods up to about 1 year. Test fluids included two different water-saturated steam environments and a mildly alkaline, saline water. The steam environments included an acid-sulfate site at the Devils Kitchen area and a neutral (pH) groundwater-diluted site at the Coso area. Test materials included mild steel, galvanized steel, 304 stainless steel, gray cast iron, 6063-T6 aluminum, cold-drawn copper, ABS and PVC plastics, and transite. Results from this study are reproduced in Figure 1.

A number of additional materials have been tested in both the acid-sulfate and groundwater-diluted steam environments, using the same test apparatus and procedures as before (Ref. 1). This report documents the results of the study conducted between February 1978 and December 1980.

TEST MATERIALS

New test materials included Duriron cast iron, 316L stainless steel, unalloyed titanium, carbon steel coated with Teflon, and glass-reinforced epoxy. Duriron is a high silicon (14.5%) gray cast iron containing about 0.95% carbon (Ref. 2). The silicon forms a very hard (480 to 520 Bhn), brittle solid solution with iron and also promotes the formation of flake graphite in the microstructure. Its presence also results in the formation of a protective surface film under oxidizing conditions. Duriron is resistant to attack by sulfuric and nitric acids, to mixtures of oxidizing acids and organic acids, and to neutral salt solutions over a wide range of temperatures (Ref. 2, 3). It is inferior to ordinary gray cast iron in resistance to alkaline solutions, and has poor resistance to sulfurous acid and to acids of the halogen family. It has very poor thermal and mechanical shock resistance, is difficult to cast or weld, and can be machined only by grinding. It is generally used in the stress-relieved condition rather than in the as-cast one. A metallographic examination of material tested in the present study showed a primary microstructure consisting of an interdendritic segregation of type-D graphite flakes in a matrix of iron-silicon ferrite solid solution. Numerous casting voids were also observed in the interior of the specimen.

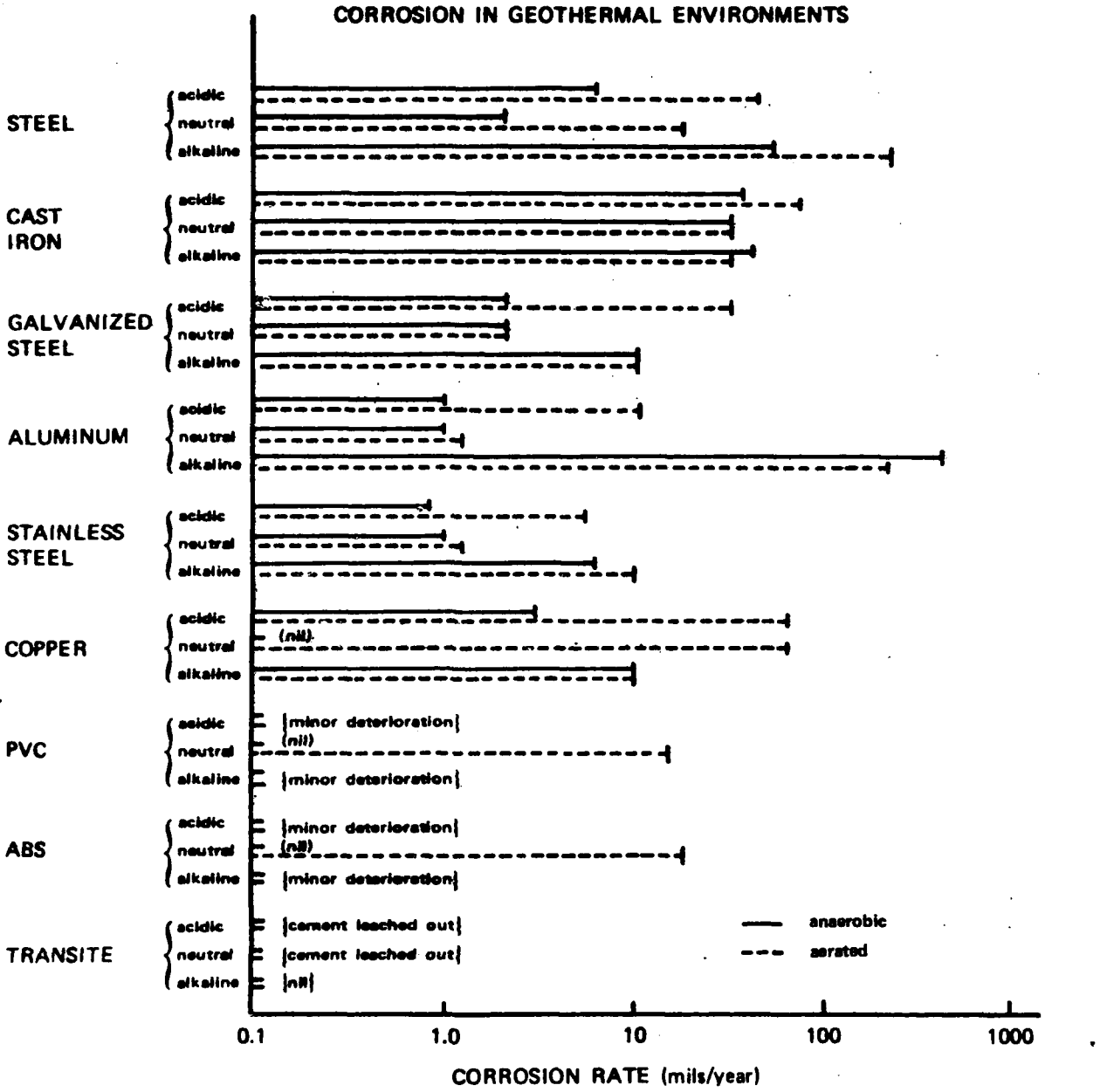

FIGURE 1. A Comparison of Corrosion Rates for Various Materials in Three Geothermal Fluids Found at the Coso Geothermal Area (Ref. 1).

The 316L stainless steel is a corrosion-resistant austenitic steel containing reduced amounts of carbon (< 0.03%) in order to make the alloy more weldable and 2 to 3% molybdenum for additional corrosion resistance. Very low carbon levels reduce the amount of chromium carbides that would form during heating of the alloy (as in welding) to insignificant levels thus maintaining the chromium level everywhere in the alloy above the minimum required for corrosion resistance. Molybdenum appears to reduce the oxidizing level required to achieve passivation and also makes a previously formed oxide film more resistant to breakdown when exposed later to a reducing solution (Ref. 4). It also lowers the chemical activity of an unpassivated alloy when exposed to a reducing solution. Moreover, it reduces the susceptibility to pitting in solutions containing halogens. The specimens tested in the present experiments consisted of Schedule 40 welded pipe in an annealed condition. The microstructure was fully austenitized and showed very minor grain boundary attack along the inner and outer surfaces.

Unalloyed titanium has excellent corrosion resistance to strongly oxidizing acids, aqueous chloride solutions, along with seawater and brines (Ref. 5), which is caused by a relatively impervious thin oxide film that readily forms on the surface in an oxygenated environment. However, it is susceptible to attack in reducing environments where the oxide film becomes unstable and cannot be repaired. In particular, it corrodes significantly in some mineral acids such as sulfuric acid (Ref. 6), which is one of the compounds present in some geothermal fluids (Ref. 1). The samples of seamless tubing tested in the present study were designated as commercially pure (99.2% Ti) ASTM B-338-73, grade 2. The microstructure consisted primarily of the acicular alpha phase, which occurs if the metal is cooled from above the beta transition temperature.

The Teflon-coated steel test specimens consisted of a 1- to 1.5-mil-thick coating of Dupont PTFE (polytetrafluorethylene) Teflon applied to the inside surface of Schedule 40 seamless steel pipe that had been previously cleaned by sand blasting. The Teflon was sprayed onto the surface, allowed to dry, then baked at approximately 750°F for about 10 minutes. The microstructure of the pipe consisted primarily of ferrite and lamellar pearlite. Its hardness was about $85R_B$ and ASTM grain size (ferrite) was estimated at 3. The ferrite along the inner surface showed some deformation consistent with that expected from the sand blasting treatment. The pipe material was estimated to be equivalent to a SAE 1050 steel meeting ASTM A120 specifications.

The glass-reinforced epoxy pipe was Bondstrand Series 2000, manufactured by Ameron, Inc. This type pipe consists of continuous glass fiber reinforcements impregnated with a black pigmented chemically resistant epoxy resin that is filament wound over a 0.020-inch-thick reinforced epoxy liner. The material is suitable for use at temperatures up to 300°F and internal pressures of 275 psi at the rated temperature. An examination of a polished section of the tested material showed both inside and outside surfaces to be generally smooth, while the interior was free of cracks but contained a large number of voids varying in diameter from 0.001 to 0.005 inch in diameter. The inner liner varied in thickness with the thinnest portions measuring about 0.012 inch.

EXPERIMENTAL PROCEDURES

The cast iron, stainless steel, carbon steel, and reinforced plastic materials were all 2-inch-diameter pipes, while the titanium was 2 1/2-inch-diameter, thin-wall (0.035 inch) tubing. In order to lower costs, samples were shorter than the 10-foot lengths tested earlier. Those tested under anaerobic conditions were 3 feet long while aerated ones were 2 feet in length. As before, aeration was achieved by cutting the pipe in half along its length and exposing one open half section to the test environment. Pipes were placed horizontally on individual supports with the anaerobic (closed) ones connected directly to individual steam outlets, while the open channels (half sections) were connected to the outlets of the comparable closed ones in order to maintain material consistency. Samples were mounted with a slight downward slope towards the outlet end to ensure a continuous drainage of steam condensate. Table 1 contains a recent chemical analysis of both condensates.

Specimens were tested continuously for approximately 17 months after which they were removed from the arrays and allowed to air dry. After drying a single ring-like sample was cut from the center of each specimen. Samples were first inspected visually using a low-power binocular microscope, and then cut into segments, mounted, and finally polished for inspection by optical microscopy.

The reinforced epoxy was cold-mounted in acrylic plastic, while metals were hot-mounted in Bakelite. The latter were also etched after polishing to reveal microstructural features. Comparisons were then made to samples of virgin (unexposed) material. Corrosion products were analyzed using x-ray diffraction techniques. Corrosion rate estimates are summarized in Table 2.

RESULTS, ACID SULFATE STEAM

DURIRON

After exposure to the anaerobic steam, the Duriron became covered with a thin (< 0.001 inch) layer of black oxidation products. An x-ray diffraction analysis showed the layer to be pyrrhotite, which is an iron-deficient iron sulfide compound of variable composition ($Fe_{0.86}S$ - FeS) (Ref. 7). In the earlier study (Ref. 1), the principal corrosion product found on the steel pipe exposed to this environment was mackinawite, an iron-rich sulfide of variable composition ($Fe_{1.057}S$ - $Fe_{1.064}S$). The reason for the difference in the corrosion products was not established, although Sardisco, et. al. (Ref. 8) and Greco and Sardisco (Ref. 9), studying an H_2S - CO_2 - H_2O - Fe system, found that pyrrhotite forms at lower H_2S concentrations (15 to 1700 ppm) than mackinawite (1700 to 66,000 ppm). Investigators have also reported that the type of sulfide compound that forms appears to depend on the initial pH of the system (Ref. 7). It is possible, then, that this difference was due to a change in the H_2S concentration and/or pH.

TABLE 1. Chemical Analysis of Corrosion Array Condensates.

Constituent/ property	Steam condensate	
	Acid sulfate	Groundwater-diluted
	ppm	
Calcium	1.3	0.5
Magnesium	<0.01	<0.01
Sodium	<0.01	0.03
Potassium	<0.1	<0.1
Hydroxide	0.0	0.0
Carbonate	0.0	0.0
Bicarbonate	<9.0	<9.0
Chloride	<1.8	<1.8
Sulfate	<5.0	<5.0
Nitrate	0.9	<0.4
Fluoride	0.02	0.02
Iron	0.25	0.16
Manganese	0.01	0.07
Arsenic	<0.01	<0.01
Copper	<0.01	<0.01
Zinc	0.09	0.01
Total dissolved solids	<15.0	<15.0
Mercury	<0.0002	<0.0002
Lithium	<0.01	<0.01
Silica as SiO_2	<1.0	<1.0
Aluminum	0.1	<0.1
Boron	0.01	<0.01
Phosphate	<0.1	<0.1
Bromide	<0.1	<0.1
Ammonium	0.25	0.80
	mg/l	
Sulfides	30.6	1.26
	mole %	
Hydrogen sulfide	1.62×10^{-3}	6.66×10^{-5}
	micromhos	
Conductivity	16.5	10.7
pH	3.13	5.8

TABLE 2. Estimates of Corrosion Rates In Structural Material Pipe Samples.

Material	Steam type		Corrosion rate, mpy	Corrosion type	Location of maximum penetration
	Acid sulfate	Groundwater-diluted			
Duriron	Anaerobic		<1		
Duriron	Anaerobic		<1		
Duriron	Aerated		<1		
Duriron	Aerated		<1		
316L Stainless steel	Anaerobic		<1		
316L Stainless steel	Aerated		<1		
Teflon-coated steel	Anaerobic		4	Pitting	Bottom
Teflon-coated steel	Aerated		4	Pitting	Side
Glass-reinforced epoxy	Anaerobic		<1		
Glass-reinforced epoxy	Aerated		4	Pitting	Side
Duriron		Anaerobic	<1		
Duriron		Anaerobic	<1		
Duriron		Aerated	<1		
Duriron		Aerated	<1		
316L Stainless steel		Anaerobic	<1		
316L Stainless steel		Aerated	<1		
Titanium		Anaerobic	<1		
Titanium		Aerated	<1		
Teflon-coated steel		Anaerobic	5	Pitting	Side
Teflon-coated steel		Aerated	8	Pitting	Bottom
Glass-reinforced epoxy		Anaerobic	<1		
Glass-reinforced epoxy		Aerated	4	Pitting	Side

The corrosion rate of the Duriron in the anaerobic acid-sulfate steam was estimated to be less than 1 mil per year (mpy). This low rate of attack might be due partly to the presence of the pyrrhotite coating, which has been shown to be more protective than mackinawite (Ref. 8).

Duriron exposed to the aerated acid sulfate steam remained essentially free of corrosion products. The corrosion rate was also judged to be extremely low (<1 mpy). This result would be expected as Duriron is very resistant to corrosion in oxidizing environments.

316L STAINLESS STEEL

The 316L stainless steel pipe showed no significant amount of corrosion in either the anaerobic or aerated acid-sulfate steam environment. In both situations, the surface of the pipe remained clean and essentially free of tarnish.

TITANIUM

The titanium samples also showed essentially no attack. The exposed surfaces appeared to be slightly more uneven than the sample of unexposed material; however, the maximum corrosion rate was estimated to be $<<1$ mpy. The surface exposed to the anaerobic steam contained patches of very thin, bluish-colored tarnish while that exposed to the aerated steam contained some brown-red stains. The latter were not identified but were probably iron oxidation products that precipitated out of the steam as a result of the aeration process and sudden reduction of pressure.

TEFLON-COATED STEEL

Samples exposed to both anaerobic and aerated fluids showed some attack of the steel. The rate of attack was about the same (4 mpy) in both environments, and consisted of small irregular pits at breaks in the Teflon coating. The sample exposed to the anaerobic fluid showed deeper pits on the bottom portion of the pipe (in the condensate channel), while the sample exposed to the aerated steam contained deeper pits on the sides (above the condensate channel) along with a layer of reddish iron oxidation products. The locations of maximum pitting were also the same in the uncoated steel pipe tested in the earlier study.

The corrosion rate of the Teflon-coated pipe in the anaerobic acid-sulfate steam was about the same (4 vs 6 mpy) as the uncoated one tested earlier; however, in the aerated steam the coated pipe showed a much lower rate (4 vs 35 mpy). In view of the type of corrosion (pitting) found on the coated pipes, any comparison of corrosion rates can be very misleading. Individual pits tend to grow at irregular rates. Growth rates can be very low for long periods of time if the pits are periodically washed by fluids. However, if they become covered over by corrosion products or other debris and form occluded cells, the remaining fluids in the bottom of the pits can acidify by hydrolytic processes leading to a rapid increase in the corrosion rate and sudden perforation of the material in a very short period of time (Ref. 10).

The mechanism causing the initial perforation of the Teflon coating was not determined. Some erosion pits were found in samples tested previously, so it is quite possible that liner erosion due to impingement by solid particles in the steam caused the initial breaks. Lorensen, et. al. (Ref. 11) observed that the Teflon PTFE coating was relatively "bumpy, rutted, or pitted" prior to exposure and attributed this to the void content resulting from the baking process.

GLASS-REINFORCED EPOXY

The glass-reinforced epoxy specimens were difficult to analyze as the inner surfaces were somewhat irregular in outline to begin with; also the thickness of the inner liner was quite variable which limited its usefulness as a marker. Moreover, the process of cutting samples from the pipes resulted in some additional damage to the surfaces. A detailed examination of the inner surfaces of both exposed and unexposed specimens were made using a low-power binocular microscope. The results of these observations are found in Appendix A.

The specimen exposed to the anaerobic steam did not appear to have suffered any significant damage. Interior surfaces were generally smooth while the wall thickness remained about the same as the original (unexposed) material. There appeared to be a slight increase in the number and size of pits found on the inner surface compared to the unexposed material (Appendix A). The interior of the wall was examined to check for an increase in void content, or other evidence of material degradation; however, nothing significant was found. Glass-fiber reinforced epoxy specimens have been shown to suffer pronounced degradation when exposed to 80°C hot water (Ref. 12). This deterioration results from the penetration of hot water into the matrix-fiber interfaces which subsequently attacks the glass-fiber surface and the interfacial coupling agent phase and leaches out glass constituent molecules. Degradation was observed as a reduction in weight, reduced tensile strength when tested after drying, by infrared measurements of the hot water medium which showed distinct traces of silica compounds and by microscopic examination, which revealed roughened and distorted fiber contours and a higher void content.

The specimen exposed to oxygenated steam showed some possible damage as the inner surface of the pipe above the condensate channel was rough and uneven, while that below the waterline was relatively smooth and appeared to be largely undamaged. A close inspection of the roughened surfaces using a binocular microscope showed a large increase in the number of pits compared to the virgin material (Appendix A). This observation suggests that wall damage may have occurred by a localized process. The maximum corrosion rate for the material above the condensate channel was estimated at 4 mpy.

RESULTS, GROUNDWATER-DILUTED STEAM

DURIRON

Only minor corrosion of the specimen exposed to the anaerobic steam took place, with the corrosion rate being estimated at $<<1$ mpy. The inner surface of the specimen was covered with a thin tarnish of a sulfurous smelling, green-gray precipitate. No analysis of the tarnish was made due to the small quantity present; however, the earlier study (Ref. 1)

found a poorly crystallized hydrated iron oxids plus an unknown compound in a similar precipitate found in an iron pipe exposed to this environment. This precipitate was believed to be due, either partly or entirely, to processes occurring upstream of the test sample as it was found in nearly all of the specimens tested.

The specimen exposed to oxygenated steam also showed only minor levels of corrosion (<1 mpy). A thin coating of reddish precipitate was found on the inside surface of the pipe. No analysis of the coating was made although it was probably iron oxidation products and was possibly due, partly, to the contaminants that were responsible for the sulfurous residue found in the pipe just upstream as was decided in the earlier study.

316L STAINLESS STEEL

The pipe exposed to anaerobic steam showed possibly very minor grain boundary attack, the rate being estimated at <<1 mpy. The bottom of the pipe (within the condensate channel) was covered with a thin black stain which was not analyzed but was believed to be due to contaminants that were carried in the steam and precipitated out. The pipe exposed to oxygenated steam also showed a very low corrosion rate (<1 mpy). The walls of this pipe were covered with a thin brownish-red stain, due to precipitation of iron contaminants that were carried in the steam.

TITANIUM

Neither titanium sample showed any significant amount of corrosion. The inside surface of the tube exposed to the anaerobic environment was coated with a thin tarnish of sulfurous-smelling precipitate, while the surface of the one exposed to the oxygenated steam was covered with a thin film of reddish-brown precipitate, as seen in other pipes.

TEFLON-COATED STEEL

The corrosion rate of the pipe exposed to the anaerobic steam was estimated at about 5 mpy, with the attack taking place at small breaks in the Teflon lining, as in the specimens exposed to the acid-sulfate steam. The rate of attack was similar to that experienced by the steel pipe tested in the earlier experiment (2 mpy). The inside surface of the pipe was covered with a thin film of the sulfurous-smelling precipitate found in the other pipes.

The oxygenated environment resulted in a slightly higher corrosion rate (8 mpy), which occurred at breaks in the Teflon lining. This rate was approximately the same as that observed on the sides of the steel pipe tested earlier, but was much less than that found in the condensate channel (17 mpy).

GLASS-REINFORCED EPOXY

Specimens tested in the groundwater-diluted steam behaved about the same as those tested in the acid sulfate steam. No significant degradation was observed in the specimen exposed to the anaerobic environment while a significant increase in surface roughness was noted on the walls, above the condensate channel, in the pipe exposed to the oxygenated steam. A sizable increase in the number of pits was found on the rougher side-wall surfaces. The corrosion rate of these surfaces was estimated at 4 mpy.

CONCLUSIONS

Unalloyed titanium and 316L stainless steel appear to be suitable candidates for use in the acid-sulfate and groundwater-diluted steam environments found at NWC, with a few qualifications. The corrosion resistance of both metals is dependent on the presence of very thin oxide films. The maintenance of these protective coverings requires an "oxygenated" environment with the oxygenating agent serving to continuously repair and rebuild the oxide layer. Any localized failures of the passive film may result in material failure by such mechanisms as pitting corrosion, crevice corrosion, intergranular corrosion and stress corrosion cracking. The added presence of chloride salts in the oxygenated fluid may prevent the oxide film from being repaired, as chloride ions will concentrate at imperfections in the film until they are able to displace the oxygen, thereby causing the film to break down at these locations. Both stainless steel and titanium are subject to pitting and crevice corrosion in oxygenated chloride environments as a result of this breakdown process.

Unalloyed titanium containing less than 0.3% oxygen is generally immune to stress corrosion cracking. Austenitic stainless steels (300 series), however, are very susceptible in chloride solutions when high stresses (applied or residual) are present in the alloy.

Ordinary 316 stainless steel may be subject to intergranular corrosion if heated into the temperature range (1000 to 1550°F) where precipitation of chromium carbides occurs. The formation of chromium carbides may lower the chromium level at grain boundaries to values below which passivity occurs (<11% Cr), rendering the grain boundaries susceptible to corrosion attack. One way to prevent the loss of passivity is to lower the carbon level in the alloy. These low carbon alloys are designated by the letter L (for example, 316L).

Because of its excellent corrosion resistance, Duriron could also be used in these two geothermal environments. Its practical use would be somewhat limited, though, because of its low resistance to thermal and mechanical shock (extreme brittleness) and because of fabrication difficulties.

The Teflon-coated steel appears to offer greatly increased resistance to corrosion compared to uncoated steel when used in the aerated steam environments assuming the rates

measured on the coated specimens are representative. In view of the type of corrosion (pitting) that occurs in this situation, additional tests should be made (perhaps by greatly increasing the exposure time) to verify these initial results.

The glass-reinforced epoxy pipe appears at first glance to be suitable for use at least in the anaerobic steam environments. However, because the visual inspection procedure used in the present study provides only limited information about this particular material, more extensive testing is probably required including weight and strength comparisons of virgin and exposed specimens. The mechanism that is responsible for increasing the surface roughness of the sides of the pipe in the aerated steam environments should also be identified.

SECTION II. CORROSION COUPON TESTING IN NAS FALLON BRINE WELL

INTRODUCTION

Materials screening tests were conducted in a deep brine well at NAS Fallon in July through December 1980. The tests utilized standard corrosion coupons of various construction materials which were suspended at the 300-foot level in the 1,700-foot deep warm well.

Testing was conducted in a planned-interval test series, (Ref. 10) which allows the determination of the metal corrosion rate for the period of exposure and any changes in the metal corrodibility or the corrosiveness of the well fluid.

A planned interval test is conducted by preparing four sets of material coupons for exposure to the environment and selecting a time period for the initial exposure. Three of the sets are placed into the test environment at zero time and set 1 is removed at the end of time interval 1. Set 2 is removed from test at time interval 2 (not necessarily time interval 1 times an integer), and set 3 is removed at time interval 3. Set 4 is then installed in test and removed in a time interval equal to the period of exposure of set 1.

The planned interval test is shown diagnammatically in Table 3.

TABLE 3. Planned-Interval Test.

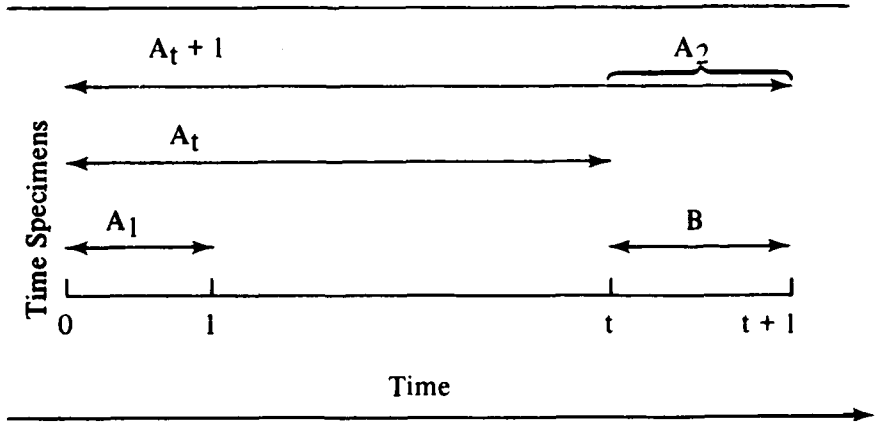

A_1, A_t, $A_t + 1$, and B represent corrosion damage experienced by test specimens in sets 1 through 4. Damage A_2 is calculated by subtracting A_t from $A_t + 1$.

WATER CHEMISTRY

Water chemistry of the test well is shown in the laboratory report in Table 4. The chloride content is 123% higher than in Coso geothermal fluids and dissolved solids are 143% higher. The pH and Cl/SO_4 ratio classify the fluid as an alkali chloride water.

TABLE 4. Well 0, NAS Fallon Water Analysis (17 December 1980).

Constituents	Parts/million
Calcium	7.5
Magnesium	10.5
Sodium	2500.0
Potassium	30.0
Hydroxide	0.0
Carbonate	150.0
Bicarbonate	1105.3
Chloride	3164.8
Sulfate	6.0
Nitrate	2.7
Fluoride	2.80
Iron	0.08
Manganese	0.07
Arsenic	0.20
Copper	0.02
Zinc	0.27
Total dissolved solids	7013.0
Mercury	<0.0002
Lithium	0.16
Silica as SiO_2	39.0
Aluminum	0.1
Boron	24.0
Phosphate	1.4
Bromide	5.3
Ammonium	4.1
Electrical conductivity, micromhos	11000.0
pH	8.8

EXPERIMENTAL PROCEDURES

Sample preparation consisted of lightly sanding the coupons to prepare a uniform surface followed by cleaning them with water, rinsing with acetone, and air drying prior to weighing the sample. The coupons were then mounted in the test rack on Teflon spacers to isolate one from another and to prevent contact with the test rack, which could set up galvanic currents, and were suspended by cable in the test well.

After exposure to the well fluid for the specified time period, the test specimens were photographed and cleaned before reweighing for weight loss determinations. Cleaning consisted of scrubbing with a hard rubber stopper under tap water to remove loose corrosion products as recommended by Fontana and Green (Ref. 10).

CORROSION RATE DETERMINATION

Corrosion rate is calculated from the weight loss of the coupon in mils per year by the equation

$$\text{mpy}^* = \frac{534\,W}{DAT}$$

where

W = weight loss, mg
D = density of specimen, g/cm^3
A = area of specimen, in^2
T = exposure time, hr

TEST RESULTS

Test results are reported in Tables 5 through 8 for 11 metals and alloys which were supplied by the Corrosion Test Supplies Co. of Baker, Louisiana. Plastic cement samples by the Brookhaven National Laboratory were also included in the tests. All materials tested, with the exception of mild steel and cast iron, exhibited less than 0.03 mpy corrosion rate, and these materials show rates of less than 2 mpy, which are acceptable in most applications. Titanium and expensive alloys are only recommended for more critical applications in aggressive environments such as in turbine materials and linings for steam separators where erosion is a major factor.

The plastic cement samples were slightly discolored or stained by the exposure to the well water, and in every case showed a gain in sample weight. The discoloration could not be removed by scrubbing and is probably a silica deposit on the cement surface. No change in thickness of the sample was measurable.

*See Reference 10.

TABLE 5. Planned-Interval Tests, NAS Fallon Well 0 (39 Days Exposure, 7 July Through 21 August 1980).

Material ASTM	Dimensions, in.		Sample weight, gms		Weight loss/gain, gms	Corrosion rate, mpy
	Diameter	Thickness	Pretest	Post Test		
Titanium B265	2,224	0.063	17.405	17.409	+0.004	0
316L Stainless A240	2.225	0.063	30.811	30.810	-0.001	0
825 Incoloy B42475	2.235	0.063	31.916	31.915	-0.001	0
625 Inconel B44375	2.240	0.063	32.558	32.560	+0.002	0
Aluminum bronze B17180	2.235	0.063	30.992	31.000	+0.008	0
Admiralty brass B11171	2.225	0.123	65.696	65.597	+0.001	0
Yellow brass B3677	2.224	0.063	33.316	33.318	+0.002	0
Deoxidized copper B152	2.245	0.068	37.426	37.428	+0.002	0
Copper B152	2.247	0.061	34.170	34.173	+0.003	0
Mild steel A285GRC	2.225	0.252	121.598	121.576	-0.022	0.17
Cast iron A74	2.230	0.196	84.349	84.318	-0.031	0.29
Brookhaven National Laboratory plastic cement sample series						
2025	2.053	0.255	31.621	31.743	+0.122	0
2034	2.048	0.252	30.967	31.060	+0.093	0
2042	2.055	0.250	27.351	27.700	+0.349	0
2052	2.025	0.253	30.148	30.216	+0.068	0
2065	2.055	0.252	25.996	26.317	+0.321	0
2071	2.061	0.252	27.641	28.354	+0.713	0

TABLE 6. Planned-Interval Tests, NAS Fallon Well 0 (73 Days Exposure, 21 July Through 2 October 1980).

Material ASTM	Dimensions, in.		Sample weight, gms		Weight loss/gain, gms	Corrosion rate, mpy
	Diameter	Thickness	Pretest	Post Test		
Titanium B265	2.224	0.063	17.397	17.400	+0.003	0
316L Stainless A240	2.225	0.063	30.764	30.761	-0.003	0.01
825 Incoloy B42475	2.235	0.063	31.427	31.422	-0.004	0.02
625 Inconel B44375	2.240	0.063	32.927	32.927	0	0
Aluminum bronze B17180	2.234	0.063	31.444	31.449	+0.005	0
Admiralty brass B11171	2.225	0.123	65.602	65.597	-0.005	0.02
Yellow brass B3677	2.225	0.063	33.172	33.170	-0.002	0.01
Deoxidized copper B152	2.242	0.067	37.380	37.375	-0.005	0.02
Copper B152	2.246	0.061	34.146	34.138	-0.008	0.03
Mild steel A285GRC	2.233	0.247	120.366	120.202	+0.164	0.69
Cast iron A74	2.230	0.195	84.309	84.162	+0.147	0.72
Brookhaven National Laboratory plastic cement sample series						
2025	2.052	0.250	31.398	31.456	+0.58	0
2034	2.052	0.251	30.753	30.827	+0.74	0
2042	2.040	0.252	27.805	27.966	+0.161	0
2052	2.026	0.252	30.205	30.242	+0.37	0
2065	2.052	0.253	27.417	27.626	+0.209	0
2071	2.060	0.277	30.200	30.690	+0.490	0

TABLE 7. Planned-Interval Tests, NAS Fallon Well 0 (109 Days Exposure, 21 July Through 7 November 1980).

Material ASTM	Dimensions, in.		Sample weight, gms		Weight loss/gain, gms	Corrosion rate, mpy
	Diameter	Thickness	Pretest	Post test		
Titanium B265	2.224	0.063	17.378	17.382	+0.004	0
316L stainless A240	2.225	0.063	30.785	30.785	0	0
825 Incoloy B42475	2.234	0.063	31.742	31.737	0.005	0.02
625 Inconel B44375	2.240	0.063	32.963	32.965	+0.002	0
Aluminum bronze B17180	2.235	0.063	31.460	31.465	+0.005	0
Admiralty brass B11171	2.224	0.123	65.743	65.737	-0.006	0.02
Yellow brass B3677	2.224	0.063	33.116	33.113	-0.003	<0.01
Deoxidized copper B152	2.244	0.066	36.967	36.964	-0.003	<0.01
Copper B152	2.245	0.061	33.444	33.432	-0.012	0.03
Mild steel A285GRC	2.232	0.252	122.962	122.453	-0.509	1.43
Cast iron A74	2.230	0.189	83.700	83.235	-0.465	1.54
Brookhaven National Laboratory plastic cement sample series						
2025	2.050	0.251	31.410	31.475	+0.065	0
2034	2.050	0.251	30.284	30.392	+0.108	0
2042	2.052	0.252	27.699	27.731	+0.032	0
2052	2.025	0.252	29.984	30.026	+0.042	0
2065	2.056	0.252	27.793	28.093	+0.300	0
2071	2.057	0.277	30.342	30.810	+0.468	0

TABLE 8. Planned-Interval Tests, NAS Fallon Well 0 (39 Days Exposure, 7 November Through 15 December 1980).

Material ASTM	Dimensions, in.		Sample weight, gms		Weight loss/gain, gms	Corrosion rate, mpy
	Diameter	Thickness	Pretest	Post test		
Titanium B265	2.222	0.064	17.398	17.399	+0.001	0
316L stainless A240	2.228	0.064	30.799	30.799	0	0
825 Incoloy B42475						
625 Inconel B44375	2.240	0.064	32.792	32.794	+0.002	0
Aluminum bronze B17180	2.036	0.065	31.214	31.210	-0.004	0.03
Admiralty brass B11171	2.230	0.123	65.761	65.762	+0.001	0
Yellow brass B3677	2.030	0.065	33.208	33.208	0	0
Deoxizided copper B152	2.044	0.068	37.437	37.435	-0.002	0.02
Copper B152	2.046	0.062	34.195	34.193	-0.003	0.02
Mild steel A285GRC	2.232	0.255	123.862	123.835	-0.027	0.20
Cast iron A74	2.232	0.191	85.225	85.189	-0.036	0.33
Brookhaven National Laboratory plastic cement sample series						
2025	2.055	0.252	31.311	31.358	+0.047	0
2034	2.056	0.250	30.383	30.500	+0.117	0
2042	2.052	0.250	27.857	27.887	+0.030	0
2052	2.040	0.255	30.456	30.466	+0.010	
2065	...	...	...	...	...	
2071	2.061	0.252	27.511	27.950	+0.439	0

Weight gain on some of the metal coupons can also be attributed to a very tightly adhering deposit that could not be removed by the cleaning method recommended. Removal of the deposit by manually scraping it off did not reveal corrosive attack under the deposit. The rate at which a deposit accumulates is influenced by the material of the surface, the concentration of the salt in the boundary layer, and the velocity of the fluid through the pipe. In this case, the fluid velocity is quite low and is due to density gradients in the well.

Table 9 compares the apparent corrosion rates of the metallic coupons with time of exposure and allows a determination to be made on the metal corrodibility and also on any change in corrosiveness of the well fluid.

Comparing damage A_1 to damage B shows the magnitude and direction of the change in corrosiveness of the fluid to the metal during the total time of test.

Comparing A_2 with B shows the magnitude and direction of change in corrodibility of the metal specimen during the test.

TABLE 9. Comparsion of Corrosion Rates in Planned-Interval Tests.

	Apparent liquid corrosiveness	Apparent metal corrodibility
	Titanium	
$A_1 = 0$ $A_t = 0$ $A_t + 1 = 0$ $A_2 = 0$ $B = 0$	No change $A_1 = B$	No change $A_2 = B$
	316L	
$A_1 = 0$ $A_t = 0.01$ $A_t + 1 = 0$ $A_2 = 0$ $B = 0$	No change $A_1 = B$	No change $A_2 = B$
	825 Incoloy	
$A_1 = 0$ $A_t = 0.02$ $A_t + 1 = 0.02$ $A_2 = 0$ $B = 0$	No change $A_1 = B$	No change $A_2 = B$
	625 Inconel	
$A_1 = 0.002$ $A_t = 0$ $A_t + 1 = 0$ $A_2 = 0$ $B = 0$	Decreased $A_1 > B$	No change $A_2 = B < A_1$

TABLE 9. (Contd.)

	Apparent liquid corrosiveness	Apparent metal corrodibility
	Aluminum bronze	
$A_1 = 0$ $A_t = 0$ $A_t + 1 = 0$ $A_2 = 0$ $B = 0.03$	Increased $A_1 < B$	Decreased $A_2 > B$
	Admiralty brass	
$A_1 = 0$ $A_t = 0.02$ $A_t + 1 = 0.02$ $A_2 = 0$ $B = 0$	Unchanged $A_1 = B$	Unchanged $A_2 = B$
	Yellow brass	
$A_1 = 0$ $A_t = 0.01$ $A_t + 1 = <0.01$ $A_2 = 0$ $B = 0$	Unchanged $A_1 = B$	Unchanged $B = A_2$
	Deoxidized copper	
$A_1 = 0$ $A_t = 0.02$ $A_t + 1 = <0.01$ $A_2 = 0$ $B = 0.02$	Increased $A_1 < B$	Increased $B < A_2$
	Copper	
$A_1 = 0$ $A_t = 0.03$ $A_t + 1 = 0.03$ $A_2 = 0$ $B = 0.02$	Increased $A_1 < B$	Increased $B < A_2$
	Mild steel	
$A_1 = 0.17$ $A_t = 0.69$ $A_t + 1 = 1.43$ $A_2 = 0.74$ $B = 0.20$	Increased $A_1 < B$	Increased $B < A_2$

TABLE 9. (Contd.)

	Apparent liquid corrosiveness	Apparent metal corrodibility
	Cast iron	
$A_1 = 0.29$ $A_t = 0.72$ $A_t + 1 = 1.54$ $A_2 = 0.22$ $B = 0.33$	Increased $A_1 < B$	Decreased $A_2 < B$

NOTE:

$A1$ = apparent corrosion rate in 39-day period
A_t = apparent corrosion rate in 73-day period
$A_t + 1$ = apparent corrosion rate in 109-day period
$A_2 = (A_t + 1) - (A_t)$
B = apparent corrosion rate in second 39-day period

No signigicant change in corrosiveness of the well fluid or in corrodibility of the metal is experienced by titanium, 316L stainless steel, 825 Incoloy, admiralty brass, and yellow brass.

Inconel 625 experienced a slight decrease in corrosiveness of the well fluid and no change in corrodibility of the metal. Aluminum bronze and cast iron experienced an increase in corrosiveness of the well fluid and a decrease in metal corrodibility. Copper, deoxidized copper, and mild steel all experienced an increase in both liquid corrosiveness and metal corrodibility.

No further geothermal fluid corrosion work will be necessary at Fallon if the RFTP is successful, since materials selection will be the responsibility of the contractor. If this is not the case and the Navy goes forward with the development on its own, then additional work will be required as reservoir fluids are developed for power and space-heating applications.

All the materials represented in the planned-interval tests would be candidates for geothermal applications at Fallon, depending on changes in the chemistry of the fluids. In general, any construction material with a corrosion rate of 5 mpy or less in a given application would be considered in an economic trade-off study.

SECTION III. AIRCRAFT ELECTRONIC AND ELECTRICAL EQUIPMENT SOAK TESTS IN DEVILS KITCHEN

INTRODUCTION

Several items of aircraft electronic and surplus electronic gear were subjected to the Devils Kitchen environment for a 25-month period. In addition, a digital clock radio and three operating battery-powered test circuits were placed in the environment and periodically removed for examination and checkout. The items were housed in a well-ventilated

target van with a wind turbine on the roof to encourage air exchange with the geothermal outside environment. The yearly mean value for hydrogen sulfide concentration in the vicinity measures 60 ppb, which is twice the California State ambient standard for area average concentrations.

EXPERIMENTAL PROCEDURES

Items and electronic gear exposed include:

A. F-9 aircraft equipment

Equipment nomenclature	Part no.
Vertical gyro indicator amplifier	105589-04-0399
Vertical gyro indicator	105759-01
DC voltage regulator	E-1597-1
Amplifier, ARA-25	AM608
Radio, UHF	505-0173-006
Receiver transmitter, radio altimeter, APN-22	02-90394-1
Altitude indicator, radio altimeter, APN-22	ID259A
Radar altimeter, APN-22	AM291
TACAN receiver-transmitter, ARN-21	RT220D
Indicator, ARN-22	ID250A
Receiver-transmitter, IFF, APX-6	RT-82C
Coder, IFF, APX-6	KY-81A

B. Surplus electronic gear

1. Microvolt-ammeter–Kintel Model 203A
2. Universal E put and timer–Beckman Model 5230
3. Two-phase oscillator–AD-YU Type 308G
4. Vector component resolver–AD-YU Type 308R2

C. Battery-powered test circuits

1. Breadboard with four integrated circuit amplifier circuits, 24-VDC schematic, Figure 2.

2. 24-VDC circuit with resistors, capacitors, and coils in parallel circuits schematic, Figure 3.
3. Solid-state timing circuit schematic, Figure 4.

D. Digital Clock Radio–General Electric Model 7-4676A

COSO TEST CIRCUITS

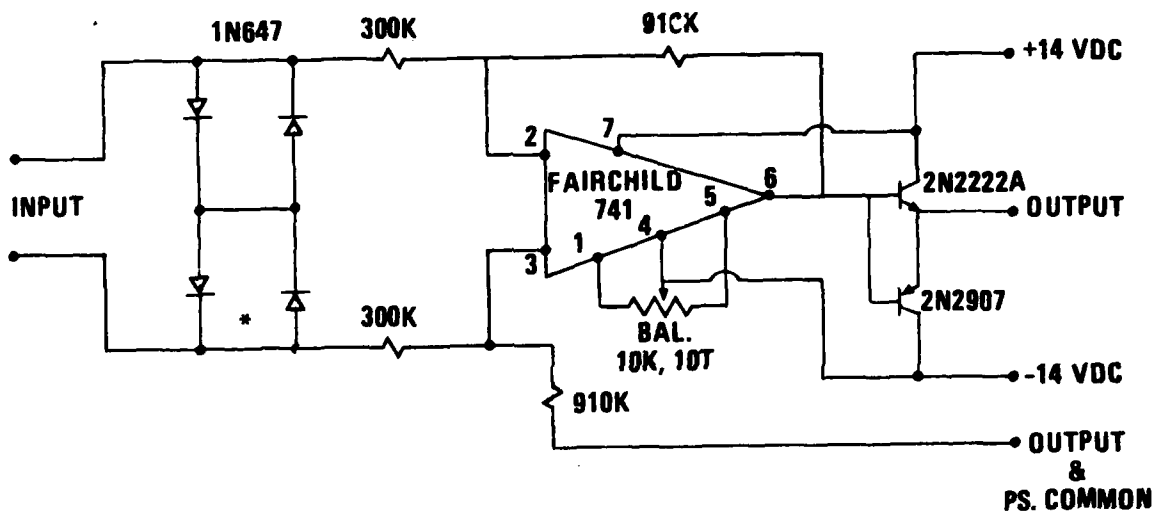

*Circuit #4 - The diode limiters on the input circuit have been removed.

Circuit test data B+ ±15 VDC, 14 mA

	Input voltage	Output
CH. #1	0.002	0.375
	0.005	1.247
CH. #2	0.002	0.567
	0.005	1.880
CH. #3	0.002	0.558
	0.005	1.500
CH. #4	0.002	0.428
	0.005	1.33.4

FIGURE 2. Breadboard with Four Integrated Circuit Amplifier Circuit.

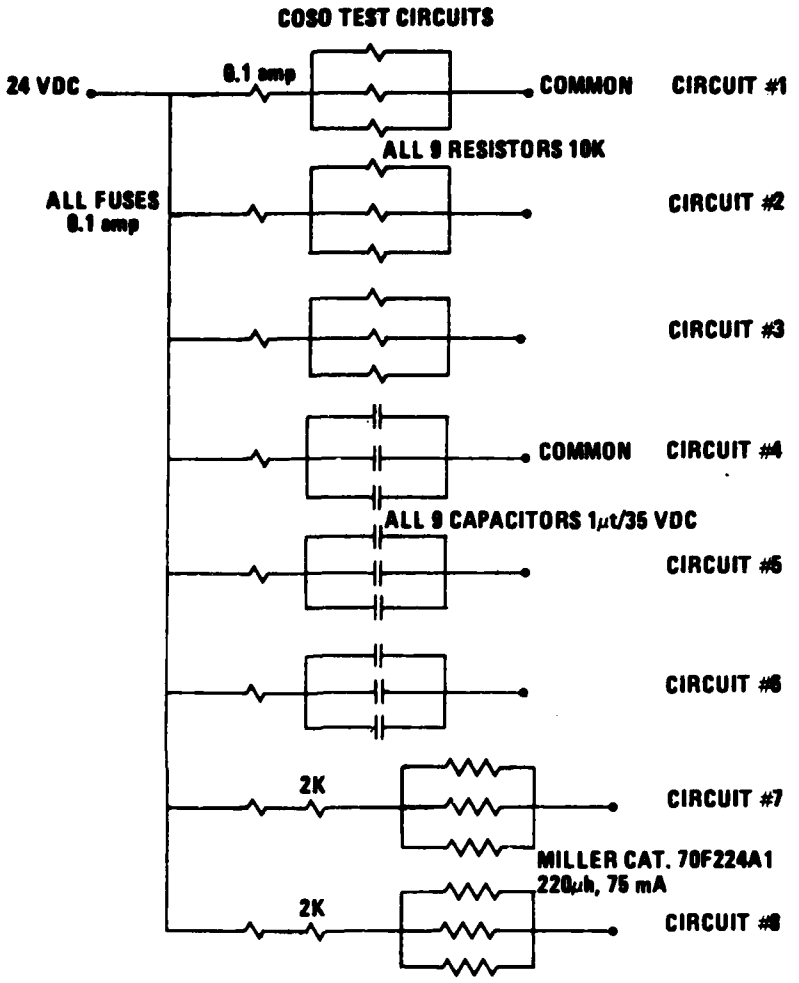

Voltage Source at 24 VDC

Circuit	Current, mA
1	7.1
2	7.2
3	0.0
4	0.0
5	0.0
6	0.0
7	12.0
8	12.0

Circuits 1, 2, 4, 5, 7 and 9—flux removed.
Circuits 3, 6 and 8 were not cleaned.

FIGURE 3. 24-VDC Circuit with Resistors, Capacitors, and Coils in Parallel Circuits.

COSO TEST CIRCUITS 20 July 1978

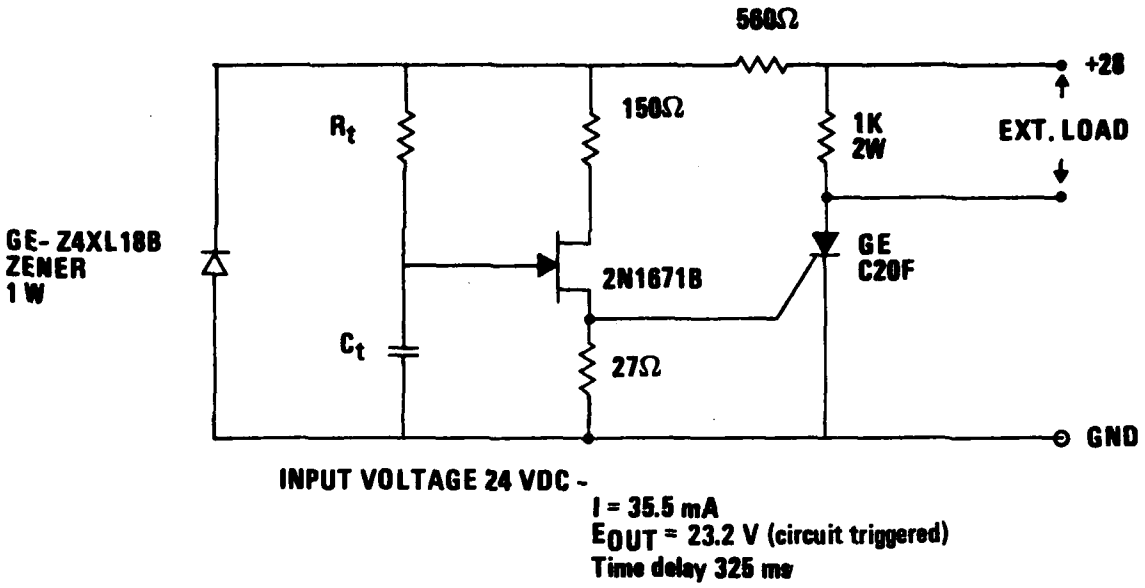

FIGURE 4. Solid-State Timing Circuit.

Code 6213 at China Lake designed the test circuits 1 through 3, and also provided technical support in bench testing all the equipment except the aircraft equipment. The aircraft equipment was bench tested by the maintenance contractor at the Naval Air Facility, China Lake.

The components in the two-phase oscillator and in the vector component resolver were not housed in protective covers, and were therefore directly exposed to the environment in the test van.

The components in the battery-powered test circuits were also unprotected by covers and directly exposed to the atmosphere in the van.

Equipment exposed to the geothermal environment was given an operational and bench test prior to and after the long-term exposure to the Devils Kitchen environment. In addition, the battery-powered test circuits, which were powered while undergoing the exposure, were removed for an intermediate check after 2 1/2 months of exposure.

TEST RESULTS

Aircraft Equipment (Period of Exposure, 11 September 1978 Through 29 October 1980)

Vertical Gyro Indicator Amplifier. This unit showed mild corrosive attack only on the screw heads which possibly had coating damage due to years of service maintenance. The amplifier was within service specifications on checkout and could have qualified as

ready for issue (RFI) equipment. The equipment performance had not been degraded due to the test environment exposure. The equipment was cleaned after checkout as is normal at this level of maintenance.

Vertical Gyro Indicator. This unit showed signs of mild corrosion only in the vicinity of the seal area. It performed within specifications on checkout and was cleaned in accordance with maintenance procedures. Performance had not been degraded due to the test environment.

DC Voltage Regulator. The regulator showed signs of corrosive attack but performed within specifications on checkout. It was cleaned and polished to high luster as required by maintenance procedures.

ARA-25 Amplifier. This unit showed no visible signs of corrosion or deterioration; all tubes checked good. Equipment was not available to bench test this gear.

Radio, UHF. The external hardware showed mild corrosive attack but no internal corrosion. The radio checked out within operational limits and had not been functionally degraded due to the environment. All functions were peaked after checkout, and the unit was cleaned, painted externally, and tagged RFI.

Receiver Transmitter, Radio Altimeter. The altimeter showed signs of hydrogen sulfide attack on silver components, part No. P-2001, and performance had been degraded by the environmental exposure. After cleaning the oxidation, the unit was within specifications and checked RFI.

Altitude Indicator, Radio Altimeter. The instrument showed mild external corrosion on case and connector pins. Cleaning connector pins and painting the case restored the instrument to RFI condition.

Radar Altimeter, APN-22. The instrument showed signs of corrosive attack due to the environment and required cleaning of silver contacts which were tarnished by hydrogen sulfide exposure. After cleaning, the altimeter required readjustment and alignment to make RFI.

TACAN Receiver-Transmitter, ARN-21. The ARN-21 would not function prior to the cleaning of corrosion products from the external connectors. Two components also required replacement, CR 801 crystals in channels 19 and 35, but the failure was probably not related to the corrosive environment as all internal components appeared free of corrosion. After alignment of the RF section, the gear was made RFI.

TACAN Indicator, ARN-21. The ARN-21 indicator showed external corrosion on the connector pins but no internal corrosion. There is a problem with the number 2 needle which has a slightly jerky movement but does not appear to be related to a corrosion

problem. The connector pins were cleaned of corrosion and the needle problem was listed on the maintenance record.

Receiver-Transmitter, IFF (Identification, Friend or Foe) APX-6. The instrument was free of internal corrosion but connector pins showed corrosive attack which required cleaning to attain proper operation. The equipment was made RFI by realigning to specifications and measuring the power levels.

Coder, IFF, APX-6. The IFF Coder required the cleaning of connector pins and the replacement of Part No. KY-81A in order to align the equipment to specifications. The part failure was probably not related to the corrosive environment.

Surplus Electronic Gear

Microvolt-Ammeter (Period of Exposure, 7 June 1978 Through 29 October 1980). Meter operates normally. No visible internal corrosion or discoloration of leads on terminals; however, external terminals and leads on power cord show evidence of sulfide attack and are black.

Universal E Put Meter and Timer (Period of Exposure, 7 June 1978 Through 29 October 1980). Meter operates normally, shows minor corrosion on some jumpers. External terminals and A/C cord plug are black from sulfide attack.

Two-Phase Oscillator, AD-YU308G (Period of Exposure, 7 June Through 29 October 1980). Operation degraded due to corrosion on external wafer switches and meter terminals. Minor discoloration on internal components.

Vector Component Resolver, AD-YU Type 308R2 (Period of Exposure, 7 June 1978 Through 29 October 1980). Equipment operates normally, no visible internal corrosion. External switches and terminals are black.

Considering the four items of equipment above, the degree of corrosive attack is influenced by the exclusion of air exchange into the instrument. Equipment with vents in the bottom of the case shows no internal corrosion or discoloration of leads or terminals. Equipment with vents on the sides of the case shows minor discoloration of leads and terminals. Uncased equipment shows definite corrosion and discoloration of leads and terminals. Silver and copper/brass components in the uncovered equipment are severely tarnished and nonplated steel screws show moderate to severe rust development.

Power cord plugs, exposed contacts, and external terminals are especially vulnerable to the hydrogen-sulfide-laden environment and would be suspect in case of equipment degradation and failure.

Battery-Powered Test Circuits

Integrated Amplifier Circuit, Figure 2. On visual inspection, both fuses and fuse holders were black as were all silver-plated terminals in the circuit. All component leads, except the gold-plated leads on the transistors and other components, had evidence of hydrogen sulfide spots beginning to form. Plated screws escaped corrosive attack, but screws with damaged plating or unplated screws showed corrosion in various stages of formation.

Changes in output voltage in the circuit at the time of bench test are shown in Table 10. Each channel check point shows a continuing reduction in output voltage with time of exposure in the corrosive environment. It was not unexpected that the circuit would exhibit some fluctuation in output because the circuit is not temperature compensated, but a continuous decrease in output voltage seems to indicate a strong influence on output due to physical changes in the circuit due to the environment.

TABLE 10. Changes in Output Voltages of Integrated Circuit With Time of Exposure to Geothermal Environment.

Channel	Input voltage	Check date and output voltage		
		20 Jul 1978	16 Oct 1978	18 Nov 1980
1	0.002	0.375	0.0945	0.00041
	0.005	1.247	0.9130	0.119
2	0.002	0.567	0.350	0.165
	0.005	1.880	1.535	0.625
3	0.002	0.558	1.162	0.0043
	0.005	1.500	1.082	0.2450
4	0.002	0.428	0.095	0.00023
	0.005	1.334	0.960	0.155

24-Volt Parallel Circuits, Figure 3. Visual inspection shows corrosion on all fuses and fuse chips and discoloration of all terminals that were cleaned of solder flux. Terminals that were not cleaned show only partial discoloration. Variation of current flow measured on bench checks in each of the eight circuits in this board are shown in Table 11 below.

TABLE 11. Current Flow Measurement in Coso Test Circuit Board.

Circuit (24-volt input)	Current flow, mA		
	20 Jul 1978	17 Oct 1978	18 Nov 1980
1	7.1	7.26	7.21
2	7.2	7.34	7.30
3	7.0	7.18	7.14
4	0.0	0.0	0.0
5	0.0	0.0	0.0
6	0.0	0.0	0.0
7	12.0	12.5	12.54
8	12.0	12.8	12.38

No significant changes in current flow are apparent in this set of circuits; therefore, circuit function would not have been impaired.

Solid-State Timing Circuit

All component leads, except gold-plated leads of transistor, show discoloration due to corrosive attack. Output voltage with 24-volt input shows only minor changes during the test period, and would not have affected circuit operation during the test. Circuit performance at three circuit checks are shown in Table 12.

TABLE 12. Timing Circuit Parameters (24-VDC Input).

Date	Output voltage, VDC	Current flow, mA
20 Jul 1978	23.2	35.5
17 Oct 1978	23.16	35.17
18 Nov 1980	22.72	35.3

Digital Clock Radio

Clock radio continues to operate normally after 25 months of exposure to the Devils Kitchen environment. Internal examination showed that the radio was free of corrosion attack; however, the electrical connector on the A/C power wire is discolored by sulfide attack.

SUMMARY

Structural materials and aircraft electronic gear have been subjected to Navy geothermal environments at the Coso Geothermal Area, Naval Weapons Center, China Lake, California and at the Naval Air Station, Fallon, Nevada.

STRUCTURAL MATERIALS

The structural materials tested at Coso in this second test series included pipe specimens of Duriron cast iron, 316L stainless steel, unalloyed titanium, carbon steel coated with Teflon, and glass-reinforced epoxy. The specimens were subjected to low-temperature steam flows from two shallow steam wells in both aerated and anaerobic flows over a 17-month time period.

Corrosion rates were less than 1 mpy in Duriron, 316L stainless, and in titanium.

Teflon-coated steel sustained corrosion rates of 4 mpy in the acid sulfate steam and 5 to 8 mpy in the ground water-diluted flow. The lower rate applies to the anaerobic section of the pipe section.

The glass-reinforced epoxy specimen sustained 1 mpy in the anaerobic section and 4 mpy in the aerated test section in both fluid types.

Standard corrosion coupons of titanium, 316L stainless steel, 825 Incoloy, 625 Inconel, aluminum bronze, admiralty brass, yellow brass, deoxidized copper, and copper suspended in a deep brine well at NAS, Fallon, Nevada sustained less than 1 mpy corrosion rate in a planned-internal test series. Mild steel and cast iron sustained maximum rates of 1.43 and 1.54 mpy, respectively, in the same test series.

Since materials selection and plant construction under request for technical proposal contract is the responsibility of the contractor, further corrosion work at Coso and NAS Fallon is not required except for in-house R&D purposes. Therefore, any additional corrosion testing of materials will be primarily to refine tests and test procedures prior to the setting up of experiments at remote Navy sites in the Imperial Valley and possibly at Adak, Alaska.

AIRCRAFT ELECTRONIC AND ELECTRICAL EQUIPMENT

A wide variety of aircraft navigational gear and standard laboratory test equipment was subjected to the geothermal gaseous emission in Devils Kitchen for long-term soak tests. Most of the equipment is in protective cases, which provide a measure of protection to the electrical circuits and minimize corrosive damage.

Corrosive attack occurred primarily to exposed connector pins, exposed terminals and jumpers, and to silver and cadmium contacts that were not completely sealed. Generally, the equipment functioned normally following exposure. In the case of the navigational equipment, cleaning of the connector pins was required before the equipment would operate within design specifications.

Older aircraft electronic equipment such as that used in this study will probably withstand the geothermal environment better than late model naval aircraft (F-14, F-16 and F-18), because in the newer aircraft more of the electronics are exposed due to the design change which now relies on cockpit pressurization to maintain the environment on the electronic gear. The electronics will now experience the same environment as the cockpit when the aircraft is parked at an air facility. If the cockpit is exposed to geothermal emissions, the electronics will suffer attack from the hydrogen sulfide.

It is recommended that some late model aircraft equipment be procured and exposed to the geysers environment with the UH-1B helicopter now in test there.

REFERENCES

1. Naval Weapons Center. *Coso Geothermal Corrosion Studies*, by Stephen A. Finegan. China Lake, Calif., NWC, Oct 1977. (NWC TP 5974, publication UNCLASSIFIED.)

2. Charles F. Walton. *Gray and Ductile Iron Castings Handbook*. Cleveland, Ohio, Gray and Ductile Iron Founders' Soc., 1971, pp. 327-31.

3. "Cast Iron" *in Metals Handbook* 8th Ed. Metals Park, Ohio, American Society for Metals, 1961. Volume 1, p. 403.

4. J. F. Mason, Jr. "Corrosion Resistance of Stainless Steels in Aqueous Solutions," in *Source Book on Stainless Steels*. American Soc. for Metals, Metals Park, Ohio, 1976, pp. 107-120.

5. I. J. Polmear. *Light Alloys: Metallurgy of the Light Metals*. American Society for Metals, Metals Park, Ohio, 1982, pp. 199-204.

6. M. S. El-Basiouny and A. A. Mazhar. "Electrochemical Behavior of Passive Layers on Titanium," *Corrosion*, Vol. 38 (5), 1982, pp. 237-240.

7. J. S. Smith and J. D. A. Miller. "Nature of Sulphides and Their Corrosive Effect on Ferrous Metals: A Review." *British Corrosion J.* Vol. 10, 1975, pp. 136-143.

8. J. B. Sardisco, W. B. Wright and E. C. Greco. "Corrosion of Iron in a H_2S - CO_2 - H_2O System, Corrosion Film Properties on Pure Iron," *Corrosion*, Vol. 19, 1963, pp. 354-359.

9. E. C. Greco and J. B. Sardisco. "Reaction Mechanisms of Iron and Steel in Hydrogen Sulfide," *Proceedings of the Third International Congress on Metallic Corrosion, Moscow, 1966, Vol. 1* (1969), pp. 130-138.

10. Mars G. Fontana and Norbert D. Greene. *Corrosion Engineering*. McGraw-Hill, New York, 1978.

11. L. E. Lorensen, C. M. Walkup and C. O. Pruneda. "Polymeric and Composite Materials for Use in Systems Utilizing Hot, Flowing Geothermal Brine III," *Geothermal Scaling and Corrosion*, ed. by L. A. Casper and T. R. Pinchbalk. Am. Soc. for Testing and Materials, 1980, pp. 164-179.

12. Ori Ishai. "Environmental Effects on Deformation, Strength, and Degradation of Unidirectional Glass-Fiber Reinforced Plastics, II. Experimetal Study," *Polymer Eng. and Science*, Vol. 15 (7), 1975, pp. 491-499.

Appendix A

GLASS-REINFORCED EPOXY SPECIMENS

I. Virgin Fiberglass Specimen (Bondstrand Fiberglass, Series 2000).

This specimen is a circular ring section sawed through a piece of the pipe. The wall thickness is 0.155 inch. There is a layer inside that is dark colored, which has a thickness of about 0.015 inch. There is a series of concentric layers about 0.015 inch each, and an outer skin. The outer skin is 0.020 to 0.025 inch thick. There are obvious voids in some of the layers where the ends of the fiberglass strands stick out. There are many voids (viewed edge-on), varying from 0.2 to 0.3 inch long, and 0.025 inch wide, and 0.010 to 0.015 inch deep. The majority of the material (viewed side-on) on this circular cut appears grayish-brown. The outer surface is dark brown (edge-on) but appears black when viewed flat-on. The inside surface layer is darker than the bulk of the material and it appears very crystalline when examined on the flat inner surface. It looks much like amber, i.e., crystalline and facetted, and is dark brown (almost like amber glass). Not many fiberglass fibers are noted on the inner surface. The inner layer is characterized by a rather smooth surface, but periodic pock-mark imperfections (pits) appear in the inner wall. The pits are generally less than 0.005 inch in diameter, and in a 0.1 x 0.1 inch area, there are probably 20 to 30 pits. The first layer of fiberglass that is visible is oriented about 60 degrees to the longitudinal axis. The fiberglass is straw-colored here. There is no resinous material in these fibers, rather resinous material surrounds the whole fiber sheath. The outer surface of the pipe is characterized by a dark reddish-black, shiny, resinous material, with the fibers again oriented about 60 degrees from the long axis, but with some randomly oriented fibers nearest the outside.

II. Corroded Specimens - Coso Test Site.

A. Closed Pipe Specimens.

The first specimen was U-shaped and located at the top half of the closed pipe array. The specimen has the same general structure as the unexposed pipe and is dark inside, sand-colored in the middle, and dark on the outside. There are some voids between layers, but not as large as in the original specimen. The inner surface of this sample shows a smooth brown resinous material with some spots ca. 0.015 to 0.020 inch square of a lighter, red-brown material. There are pieces that are torn out from the sawing process. It is obvious from this specimen that there are random fiberglass fibers in the inner dark material layer. There are also sizably

larger voids (pits) on the inner surface than in the unexposed specimen. The frequency is about the same as the previous specimen but the pits seem to be larger (0.005 to 0.155 inch). There is some inner layer separation from the base matrix where the measured thickness of the inner layer is 0.015 to 0.018 inch and the outer layer is thinner (0.012 to 0.016 inch). It is of note that the material that was exposed to the corrosive fluid is a different color on both the inside and the outside than the unexposed specimen. The unexposed specimen was glossy black on the outside, whereas the exposed material is a dull black, suggesting that some of the material has been stripped away. More fibers are showing on the outside. The exposed specimen appears to have increased in thickness by a few thousandths of an inch, perhaps by water absorption through the pinholes.

Next, three smaller specimens were examined. The first of these was coded "T", meaning top of the closed pipe array. The inner surface is a brownish translucent material showing random fiberglass fibers. Pitholes are also present but not so frequent as in the previous specimen. They are longer, however (0.005 to 0.007 inch in diameter). There is evidence of clay, dust and dirt inside the specimen. Also reddish resinous material in the 0.010 x 0.015 inch patches. The edges of the specimen are damaged due to sawing and laminated as above. Pinholes are noted between the layers. Some longitudinal sections were torn loose from the inner surface. The different layers alternate colors–dark, light, etc. The specimen wall thickness is 0.155 inch.

The next specimen is the middle section (side) of the closed pipe. The back part of the specimen shows evidence of leaching away, leaving exposed fiberglass fibers. The layers are variously colored as above. The brown layers appear to have holes in them (edge-on). There is some cracking of the inner layer (saw cuts?). There is a larger fraction of voids than in the top specimen (average size 0.007 inch). In one 0.1 x 0.1 inch area, there is an interesting patch beneath one pinhole on the inner surface, where it appears that the fluid ran into the inside of the inner layer. The pinhole is about 0.005 inch in diameter and the infused area is 0.050 x 0.075 inch. There is also evidence of clay-like material and red resinous material seen before.

The last specimen in this series was from the bottom of the closed tube. Looking at the outside of the closed tube specimen, it is still shiny and black and does not appear to have been corroded away. The fibers are still imbedded in the black matrix. The inner layer is damaged somewhat (sawing). There is a considerably thicker layer of mixed resinous material and the clay-like material than on either the top or the side specimens. There is a greater number of larger perforations–some as large as 0.01 x 0.01 inch. In a particular 0.1 x 0.1 inch area, there were 30 to 40 pits, of which 10 are larger than 0.01 inch in diameter. One can see the fibers imbedded in the inner layer, also a few resinous spots. There is a crack on the inside (sawing?), but otherwise there is good bonding between the layers with no large voids between them. The total thickness of the pipe wall is 0.155 ± 0.005 inch.

B. Open Pipe Specimens

There are three specimens from the open pipe section–two side sections and a bottom section. The most remarkable thing about these specimens is the complete layer of

light brown material spread over the inside. Also, there are a tremendous number of medium-sized (0.005 to 0.007 inch) pits, and indented fiber markings. Scraping a 0.1 x 0.1 inch area, one sees a tremendous number of pits into the matrix (ca. 100), and the lines where the fibers apparently were. The light brown material filled these depressions. The brown microcrystalline layer is not terribly thick (0.001 to 0.002 inch), but the tremendous number of pits is notable.

Looking at the saw cut side-on, the whole side section specimen is uniformly grayish, and not nearly so torn up as the previous specimens. On the back surface, we see two different effects. Where the matrix is visible, there is shiny black matrix with enclosed fibers, but where there is adherent, red, mud-like material, the fibers are all exposed and the matrix is damaged. Looking at the opposite edge, edge-on, there are no interlayer voids. The thickness is nominally 0.014 inch—apparently it has shrunk a bit.

The sample from the opposite side of the open pipe appears to duplicate the one above. There is again the brown adherent layer, with some fibers sticking up through the brown material and a large number of pits. The integrity of the layers seems good - no large interlayer separations. The outside edges show the shiny black material with the encapsulated fibers, and an area covered with the brown crystalline material where the black matrix is gone and where fibers are sticking up out of the matrix. (This area is at the top edge of the open section.) The edge-top is also open to the air and shows the brownish microcrystallinity. Various layers have expanded or contracted relative to each other, but no splits are noted down in between the layers.

Last, is the bottom specimen of the open tube. This section forms the base of the channel. The back of it shows a dull black material, but all the fibers are still embedded and there is no apparent deposit on it. The material is integral and well bonded together—with color distinction between the layers. The inner layer is dark glossy brown. If one looks at the inner surface at one of the edges, there are some pits covered by the brown microcrystalline material and some fibers sticking up through this layer. In addition, a few of the pits contain rock-like projections. On viewing these at increased magnification, protrusions are evident. When one protrusion was removed, it seemed to be resinous -dark red amber resin. It is just like the inner layer matrix, and seems to have penetrated up through the pits. Down the center of the specimen is a reddish-brown material--darker than the tan higher up on the sides. The number of pits seems to be fewer, but the sediment layer is thicker as well. There is one crack (sawing?) running across the specimen. The red-brown material in the center is 0.002 to 0.004 inch thick. Scraping away a section of it, one sees that there are not a great number of pits underneath it either. There are really fewer pits into the matrix below this red material. In a 0.10 x 0.10 inch area there are only 10 to 15 pits (with average diameter of 0.003 to 0.004 inch in most cases). The material examined was installed on February 3, 1978.

III. Corroded Specimens - Devils Kitchen Test Site.

A. Closed Pipe Specimens

The first specimen in this series is a U-shaped top-half section of the closed pipe. The back of the specimen is very damaged. It is dull black in appearance and has lots of loose fibers on the outside at 60 degrees to the longitudinal axis of the pipe. In some areas of the pipe, there are two exposed layers at 90 degrees to each other. The edge view shows a typical dark inner layer and several composite layers alternating light and dark out to the outside surface. A few separations between layers are noted. Examining the inner layer side-on, there are voids noted in the inner layer matrix. The voids are down inside the matrix—different from Coso specimens. There is a dark red-brown stripe at the edge (3 o'clock when viewed front-on). The inside layer is translucent and one can see some of the fibers down through the matrix. Also, some red resinous patches 0.02 x 0.02 inch. There is a considerable number of large perforations. At top dead center, there is an area where something appears to have penetrated the pitholes down into the matrix. It is shinier and darker than the rest of the matrix. There are more red-brown resinous areas, some quite large, and a few areas where material has penetrated the matrix. At the opposite edge (9 o'clock) there are 20 to 30 perforations with 50% being larger (0.010 to 0.015 inch in diameter) than the others. This specimen has survived the sawing operation well. There are remarkably well-bonded layers.

Next, three smaller specimens were studied—one each from the top, middle, and bottom of the pipe. The sample from the top of the closed specimen shows a characteristic light, red-brown haze over the inside but not thick enough to obscure one's view of the fibers embedded in the surface. There are quite a few red resinous deposits on this specimen—three in one 0.01 x 0.01 inch area. There are perforations down into the inner surface and throughout the inner layer (side-view). The back is severely damaged—with many fibers sticking out and no shiny matrix left. There are some interlayer separations.

The next specimen is the mid-section. There are fewer inner surface pits. Some saw damage (tearing) is noted across the specimen. A few red resinous deposits are noted. The layers are well-bonded. The black sheen on the back has disappeared but the fibers are still well-bonded.

On the piece from the bottom of the closed section, the back is well-preserved and shiny. Fibers are all embedded. There is disbondment of the outer layer and perforations between the various layers. On the inside surface, there is a reddish-brown stain on the edge. There are some perforations here. An area on the center of the specimen shows electrolyte intrusion through the pits. The number of pits is not large. Near the reddish-brown stain there are a few very large pits (0.010 to 0.015 inch). There is a little of the red-brown resinous material at the edge where intrusion took place. One can see the embedded fibers, but there is a brown tinge over the inner surface.

B. Open Pipe Specimens

Three specimens were examined—two from the sides and one from the bottom of the open section. In the first side piece, the part that was pointed upward exposed to the atmosphere shows six layers including inner and outer, and the fibers are frayed (fuzzy looking). There is an interlayer separation next to the outer layer. Looking at the sawed edge, it seems pretty well bonded—only a few small interlayer perforations. Looking at the back of the specimen, the matrix is completely removed from the exposed upper edge—and shows only exposed fibers. As we move down from the exposed edge, fibers still stick out, but there is a powdery-looking oxidized matrix. Toward the center of the specimen back, there is some crystalline material attached that is not of matrix origin. At the bottom of the specimen, the black matrix is intact and there is some sandy, clay-like material attached. Looking at the inside surface, it seems similar to the Coso specimens. The top edge is dark brown and there is particulate matter attached, numerous perforations and free strands of fibers in all directions. Progressing down the specimen, the covering gets more red and the pits decrease in size. There is a deep, red-brown stain toward the bottom of this specimen.

Looking at the opposite side specimen, there is an exposed edge which is whitish and in which the bonding material is depleted to a depth of 0.020 inch. There is some disbonding of the layers towards this edge. The back shows the same characteristics as in the previous specimen. The brown porous material noted look like ion exchange resin on high magnification and are distinctly separate from the glass fibers. They appear to have originally been part of the glossy black matrix. Toward the center of this specimen, there is a large deposit of white and brown material, which on higher magnification looks like oxidized black matrix with salt deposits in between. At the bottom of the outside layer on this specimen, there is a brown friable material that gives appearance of clay. The inside layer is a dark, highly porous, purple material at the top edge. Pits are very numerous. The middle inside portion shows larger pits. It appears that the matrix has been selectively dissolved or oxidized and what is left is a "furry-looking" matrix with sand or silica embedded in it. There are a large number of pores and free fibers sticking out. As we progress toward the bottom of this specimen, the pits decrease in size and number. The parts exposed to air have larger pits and more of them. On higher magnification, the furry-looking matrix with some particles embedded in it is seen. This specimen also gets distinctly redder towards the bottom.

The last specimen in this series is from the bottom of the open section. Looking at the outside first, we see that overall, although there are stains on it, the material has not disbonded at all, and that indeed the black shiny material is present overall. Looking at the saw cut edges, one can see some internal voids in the inner layer. There is also some slight disbonding of the layers. Looking at the inside surface, at each upper edge the material attached is definitely red, and there are deep pits on one side. In a 0.10 x 0.10 inch area, there are about 30 pits, 0.020 to 0.025 x 0.010 inch each. One side shows slightly more pitting than the other. Toward the center of this specimen one can see an area where the scale has fallen off and only a few perforations. Here, in a particular 0.10 x 0.10 inch area, three to five very small pits are seen (0.003 to 0.005 inch in diameter). One can see fibers through the binder which are well-bonded. There is no layer disbonding. The inner matrix is dark amber and is in pretty good condition. It is apparent that air is needed for deep, dark colored pitting to occur.

INITIAL DISTRIBUTION

4 Naval Air Systems Command
- AIR-00D4 (2)
- AIR-01A (1)
- AIR-4106B (1)

2 Chief of Naval Operations
- OP-413F (1)
- OP-45 (1)

2 Chief of Naval Material
- MAT-08E, Cdr. Clark (1)
- MAT-05 (1)

7 Naval Facilities Engineering Command, Alexandria
- FAC-03 (1)
- FAC-032E (1)
- FAC-04 (1)
- FAC-08T (1)
- FAC-09B (1)
- FAC-111 (1)
- FAC-1113 (1)

1 Naval Facilities Engineering Command, Atlantic Division, Norfolk (Utilities Division)

1 Naval Facilities Engineering Command, Chesapeake Division (Maintenance and Utilities Division)

1 Naval Facilities Engineering Command, Northern Division, Philadelphia (Utilities Division)

1 Naval Facilities Engineering Command, Pacific Division, Pearl Harbor (Utilities Division)

1 Naval Facilities Engineering Command, Southern Division, Charleston (Utilities Division)

5 Naval Facilities Engineering Command, Western Division, San Bruno
- Code 09B (1)
- Code 09C3 (1)
- Code 11 (1)
- Code 112 (1)
- Code 24 (1)

4 Naval Sea Systems Command
- SEA-05R13 (1)
- SEA-04H3 (1)
- SEA-99612 (2)

1 Commander in Chief, U.S. Pacific Fleet (Code 325)

1 Headquarters, U.S. Marine Corps

1 Commander, Third Fleet, Pearl Harbor

1 Commander, Seventh Fleet, San Francisco

1 Naval Academy, Annapolis (Library)

3 Naval Civil Engineering Laboratory, Port Hueneme
- Commanding Officer (1)
- LO3AE, Dave Holmes (1)
- Technical Library (1)

2 Naval Energy & Environmental Support Activity, Port Hueneme
- Code 11011 (1)
- Code 111A (1)

1 Naval Postgraduate School, Monterey (Library)

3 Naval Ship Weapon Systems Engineering Station, Port Hueneme
Code 5711, Repository (2)
Code 5712 (1)
1 Naval War College, Newport
1 Headquarters, U.S. Army (DALO-TSE)
1 Chief of Engineers (DAEN-MPZ-E)
1 Construction Engineering Research Laboratory, Champaign (CERL-ES)
1 Facilities Engineer Support Agency, Ft. Belvoir (FESA-TE)
1 Headquarters, U.S. Air Force (AF/LEY)
1 Air Force Systems Command, Andrews Air Force Base (AFSC/DEE)
2 Air Force Academy
Code LGSF (1)
Library (1)
1 Air Force Wright Aeronautical Laboratories, Wright-Patterson Air Force Base (AFWAL/POOC)
1 Civil Engineering Center, Tyndall Air Force Base (DEB)
1 McClellan Air Force Base, (SMAL/XRE)
12 Defense Technical Information Center
1 Bureau of Mines, Reno, NV
1 Department of Energy, San Francisco Operations, Oakland, CA (J. Crawford)
1 General Services Administration, Public Buildings Service (Energy Conservation Division)
5 United States Geological Survey, Menlo Park, CA
Dr. Bacon (1)
Dr. Christianson (1)
Dr. Duffield (1)
Reid Stone (1)
Library (1)
1 Associated Universities, Inc., Upton, NY (Brookhaven National Laboratory)
1 California Department of Conservation, Sacramento, CA
1 California Department of Water Resources, Sacramento CA
1 California Division of Mines and Geology, Sacramento CA
1 California Energy Resources Conservation and Development Commission, Sacramento, CA
1 California State Land Division, Sacramento, CA
1 Geothermal Resources Council, Davis, CA
1 Johns Hopkins University, Applied Physics Laboratory, Laurel, MD
1 Lawrence Berkeley Laboratory, Berkeley, CA
1 Los Alamos National Laboratory, Los Alamos, NM (Reports Library)
1 Oak Ridge National Laboratory, Oak Ridge, TN (Energy Division)
1 San Diego Gas & Electric Company, San Diego, CA (Otto Hirr)
1 University of Hawaii, Honolulu, HI (Institute of Geophysics)
3 University of Utah, Salt Lake City, UT
Department of Geology, Dr. J.A. Whelan (1)
Earth Science Laboratory, H. P. Ross (1)
Geology & Geophysics Library (1)
1 University of Utah Research Institute, Salt Lake City, UT (Earth Sciences Group)

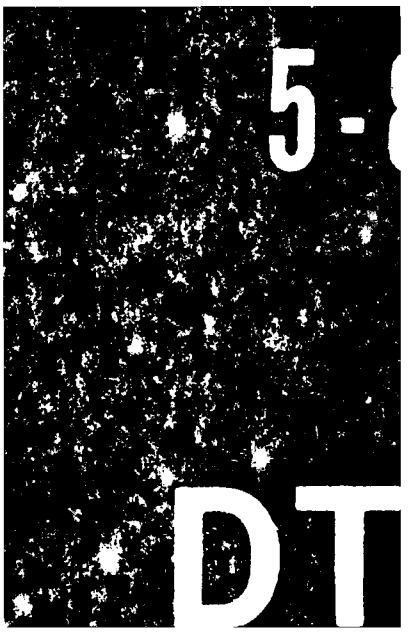
5-
DT